

Experimental Preparation of High NOON States for Phonons

Junhua Zhang^{1*}, Mark Um¹, Dingshun Lv¹, Jing-Ning Zhang¹,
Lu-Ming Duan^{1,2} and Kihwan Kim¹

¹Center for Quantum Information, Institute for Interdisciplinary Information Sciences, Tsinghua University, Beijing, 100084, P. R. China

²Department of Physics, University of Michigan, Ann Arbor, Michigan 48109, USA

Multi-party entangled states have important applications in quantum metrology and quantum computation. Experimental preparation of large entangled state, in particular, the NOON states, however, remains challenging as the particle number N increases. Here we develop a deterministic method to generate arbitrarily high NOON states for phonons and experimentally create the states up to $N = 9$ phonons in two radial modes of a single trapped $^{171}\text{Yb}^+$ ion. We demonstrate that the fidelity of the NOON states are significantly above the classical limit by measuring the interference contrast and the population through the projective phonon measurement of two motional modes. We also measure the quantum Fisher information of the generated NOON state and observe the Heisenberg scaling in the lower bounds of the phase sensitivity as the N increases. Our scheme is generic and applicable to other photonic or phononic systems.

INTRODUCTION

Entanglement is an essential resource for quantum computation and quantum metrology. Classically, a parameter can be estimated more precisely by using more particles in the measurement, and the reduction of the statistical error is proportional to the square root of the particle number. In quantum metrology, the reduction factor can be improved to be linearly proportional to the particle number, which is called the Heisenberg limit, by using many-particle entangled states. The ultimate Heisenberg limit can be achieved with the NOON state for identical bosons [1, 2], which can be understood by the superposition of two modes with only one of them occupied by N bosons. The NOON state has the form [3]

$$|\psi_{\text{NOON}}\rangle = \frac{1}{\sqrt{2}} (|N, 0\rangle + e^{iN\varphi_S} |0, N\rangle), \quad (1)$$

where the relative phase φ_S between two modes is linearly proportional to N , showing the Heisenberg scaling for parameter estimation through the interferometric measurement. For photonic systems, experiments have demonstrated NOON states with particle numbers up to $N = 5$ [4–11]. For distinguishable particles, up to 10 photons and 14 ions have been prepared into the closely-related GHZ states [12, 13]. NOON states have also been demonstrated in nuclear spins (NMR) [14], atomic spin waves [15], and microwave photons in superconducting systems [16].

On the other hand, the quantized vibrational modes of ions in a harmonic trap have recently received increasing attention beyond the standard role as the mediator of quantum operations between internal states of ions. Phonons, bosonic quasiparticles, which represent the number of quantized excitations of a vibrational mode [17, 18], are proposed as the information carrier for quantum simulation [19, 20], Boson sampling [21], and quantum computation with continuous variables [22]. Recently, the NOON state with $N = 2$ has been generated through interference of phonons in each localized harmonic potential [23]. The phonons in the trapped ion system can also be manipulated through the interaction with the internal

degree of freedom of an atom, similar to manipulating photons through an atom in a cavity [24]. Here, we develop a generic and deterministic scheme to generate phononic NOON states with arbitrary number of bosons N for any two vibrational modes of ions based on anti-Jaynes-Cummings coupling. We experimentally generate the NOON state with phonon numbers up to $N = 9$ and clearly observe the Heisenberg scaling in the lower bound of the sensitivity in the phase estimation provided by the quantum Fisher information of the state. This phononic NOON state can be applied to the precision measurement of Force or electric field gradient.

RESULTS

Experimental Setup

In experiment, we generate the NOON state in two radial modes of an $^{171}\text{Yb}^+$ ion trapped in a standard Paul trap as shown in Fig. 1(a). We note that our realization is directly applicable to any normal modes of multiple ions. The two radial modes are denoted as X and Y, with trap frequencies $\omega_X = (2\pi)3.2$ MHz, $\omega_Y = (2\pi)2.6$ MHz and Lamb-Dicke parameters $\eta_X = \Delta k \sqrt{\frac{\hbar}{2M\omega_X}} = 0.0538$, $\eta_Y = 0.0597$, where Δk is the difference of the wave vector of two perpendicular Raman laser beams, M is the mass of a single $^{171}\text{Yb}^+$ ion. To mediate phonon operations, two hyperfine levels of the $^{171}\text{Yb}^+$ ion in the $^2S_{1/2}$ manifold are used as a qubit, denoted as $|\downarrow\rangle \equiv |F=0, m_F=0\rangle$ and $|\uparrow\rangle \equiv |F=1, m_F=0\rangle$, which is separated by the hyperfine frequency $\omega_{\text{HF}} = (2\pi)12.6428$ GHz. The state of the system is represented in Fock state basis as $|\sigma, n_X, n_Y\rangle$, where σ is the state of the qubit and n_X, n_Y are the phonon numbers in each mode. Two laser beams from a pico-second pulsed laser with the wavelength of 355 nm are used to generate a stimulated Raman process to drive the carrier transition and motional sideband transitions of the ion [25].

We operate the motional degrees of freedom with the combination of carrier and blue-sideband pulses described by the

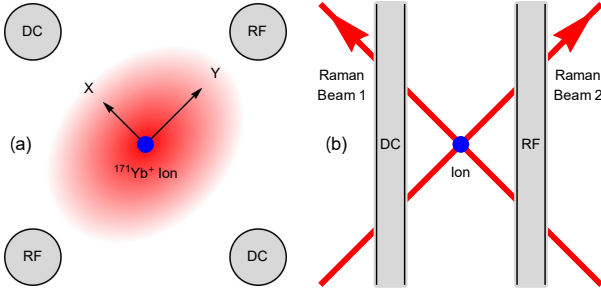


FIG. 1. **Experimental setup.** (a) Side view and (b) top view of the trap and laser configuration.

time evolution of the following interacting Hamiltonians of H_C and H_M , respectively [18]:

$$H_C = \frac{\Omega_C}{2} (\sigma^+ + \sigma^-), \quad (2)$$

$$H_M = \frac{i\eta_M \Omega_M}{2} \left(e^{i\varphi_M} \sigma^+ a_M^\dagger - e^{-i\varphi_M} \sigma^- a_M \right), \quad M = X, Y,$$

where Ω_C and $\eta_M \Omega_M$ are the Rabi frequencies of carrier and blue sideband transitions, φ_M is the phase of the driving signal, $\sigma^+ = |\uparrow\rangle\langle\downarrow|$ and $\sigma^- = |\downarrow\rangle\langle\uparrow|$, and a_M^\dagger (a_M) is the creation (annihilation) operator of the motional mode M (see also Methods, Hamiltonian of the System).

Generation Sequence

In Fig. 2, we illustrate the pulse sequence for the generation of NOON state of $N = 3$, which is $|3, 0\rangle + |0, 3\rangle$, as an example (See Methods, Pulse Sequence for a generalized description of the pulse sequence). We first initialize the state to $|\downarrow, n_X = 0, n_Y = 0\rangle$ by the standard optical pumping technique and the ground state cooling of both motional modes using the Doppler cooling followed by the resolved Raman-sideband cooling. Then we transfer the initial state $|\downarrow, 0, 0\rangle$ to $|\downarrow, 1, 1\rangle$ by applying successive π -pulses of blue-sideband and carrier transitions. A $\frac{\pi}{2}$ -pulse of blue-sideband transition on the X mode is applied to change the state to $|\uparrow, 2, 1\rangle + |\downarrow, 1, 1\rangle$. Finally, two composite-pulse operations followed by a blue-sideband π -pulse on Y mode and a carrier π -pulse are performed to generate the state $|\downarrow, 3, 0\rangle + |\downarrow, 0, 3\rangle$. The composite-pulse schemes are inspired by Ref. [26] and are capable of driving π -transitions of blue sideband on two different phonon number states, which have different Rabi frequencies (See Methods, Pulse Sequence). In order to improve the fidelity of the state, pulse-shaping technique is applied to all blue-sideband pulses to suppress various off-resonant couplings (See Methods, Pulse Shaping). With the pulse sequence, we generate the NOON state up to $N = 9$ which is mainly limited by experimental imperfections that will be discussed later.

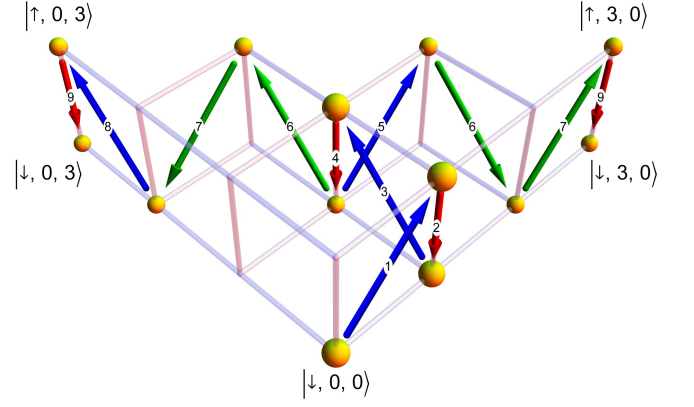


FIG. 2. **Generation sequence of the NOON state of $N = 3$.** The blue arrows indicate blue-sideband transitions, the red arrows indicate carrier transitions and the green arrows indicate composite-pulse operations. The numbers on the arrows denote the order of the operations.

Phase Sensitivity

We observe the sensitivity of the phase estimation with the NOON states increases as the number of phonons N increases. The phase between X and Y modes can be measured by the interference through the beam splitting operation. For photons, the creation and annihilation operators of output paths after the beam splitting operation are described by linear combinations of those for input paths. For phonons, we can define similar output modes written as

$$a_O^\dagger = a_X^\dagger \cos \theta + e^{i\varphi} a_Y^\dagger \sin \theta, \\ a_O = a_X \cos \theta + e^{-i\varphi} a_Y \sin \theta. \quad (3)$$

In the experiment, the parity, $\Pi = \exp[i\pi a_O^\dagger a_O]$, of the generated state is measured in the output modes with $\theta = \pi/4$. Depending on the value of φ , we observe the oscillation of the parity described as

$$\langle \Pi(\varphi) \rangle = C_P \cos N\varphi. \quad (4)$$

Fig. 3(a) shows the experimental results of the parity oscillations from $N = 1$ to $N = 9$ of the generated NOON states. As shown in the fitting parameter k , the enhancement of the phase sensitivity is in agree with N within 2.6% deviation. As N increases, the contrast C_P decreases due to experimental imperfections. However, it is clearly shown that up to $N = 9$, the contrast is over 0.5, which indicates the existence of quantum entanglement in the state.

The phonon distribution, and furthermore parity, of the output mode in Eq. (3) is measured through observing the time evolution of blue-sideband transition of that mode and then fitting the fluorescence signal [18]. The excitation of the output mode (3) is realized through driving the blue-sideband transition of X and Y modes simultaneously shown as

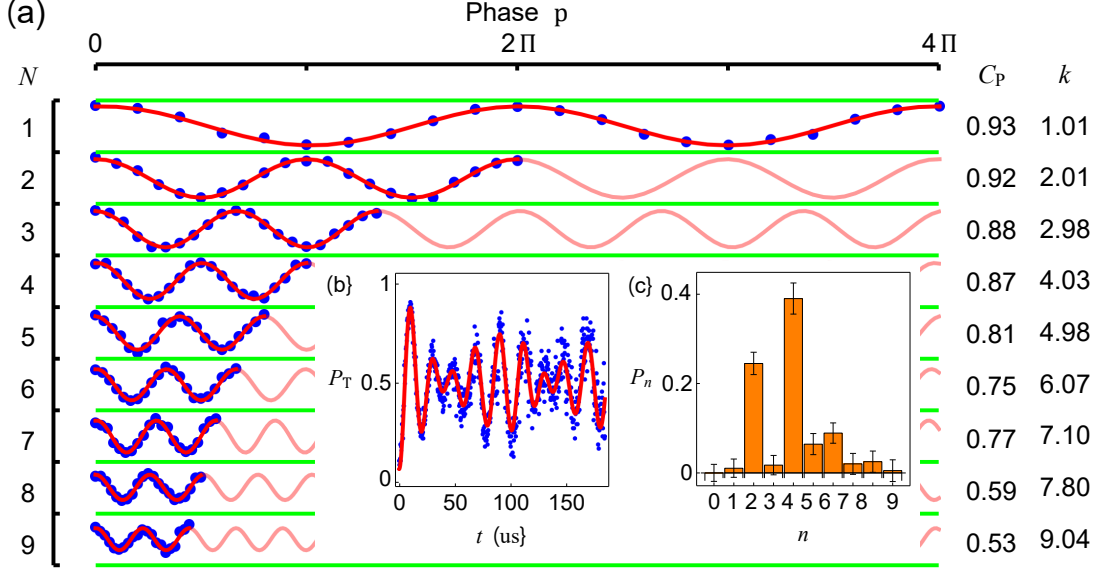


FIG. 3. **Parity oscillations of the generated NOON states from $N = 1$ to $N = 9$.** (a) The blue dots are experimental data, and the red lines are fitting curves with $\langle \Pi(\varphi) \rangle = A \cos k\varphi + B \sin k\varphi + C$, and $C_P = \sqrt{A^2 + B^2}$. (b) The blue-sideband fluorescence signal of the output mode with $\varphi = 0$ for the NOON state of $N = 7$ and its fitting with $P_T(t) = A - \frac{1}{2} \sum_n P_n \exp[-(n+1)^{0.7} \lambda t] \cos[\mathcal{L}_n^1(\eta^2) \Omega t / \sqrt{n+1}]$, in which A , P_n , λ , η and Ω are fitting parameters. (c) The corresponding phonon distribution P_n . We note that generally $\sum_n P_n < 1$ due to the experimental errors in the generation stage. The error bars are derived from fitting error with a confidential level of 0.95 through out the manuscript.

$$H_O = H_X + H_Y = \frac{i\eta_X \Omega_X}{2} (\sigma^+ a_X^\dagger - \sigma^- a_X) + \frac{i\eta_Y \Omega_Y}{2} (e^{i\varphi} \sigma^+ a_Y^\dagger - e^{-i\varphi} \sigma^- a_Y). \quad (5)$$

By setting $\sqrt{2}\eta_X \Omega_X = \sqrt{2}\eta_Y \Omega_Y \equiv \Omega_O$, we can obtain the effective Hamiltonian for the output mode excitation as

$$\begin{aligned} H_O &= \frac{i\Omega_O}{2\sqrt{2}} \left[\sigma^+ (a_X^\dagger + e^{i\varphi} a_Y^\dagger) - \sigma^- (a_X + e^{-i\varphi} a_Y) \right] \\ &= \frac{i\Omega_O}{2} (\sigma^+ a_O^\dagger - \sigma^- a_O). \end{aligned} \quad (6)$$

Fig. 3(b) shows a typical time evolution of the blue-sideband excitation of the output mode (3) with $\varphi = 0$ and Fig. 3(c) shows the phonon number distribution by fitting the time evolution for the NOON state of $N = 7$. The phase of the generated state ϕ_S is carefully measured and aligned with the output mode of $\varphi = 0$ (see Methods, Phase Alignment).

Fidelity and Population Measurement

We also measure the fidelity $F \equiv \langle \psi_{\text{NOON}} | \rho_{\text{exp}} | \psi_{\text{NOON}} \rangle$ of the generated NOON state. Since the density matrix of an ideal NOON state contains only two diagonal terms and two off-diagonal terms, the fidelity can be obtained by directly measuring these terms. The off-diagonal terms are proportional to the contrast of the parity oscillation $C_P = 2 |\langle N, 0 | \rho_{\text{exp}} | 0, N \rangle|$ (see Methods, Fidelity Analysis). For

the measurement of diagonal terms, i.e., the population of $|\downarrow, N, 0\rangle$ and $|\downarrow, 0, N\rangle$, we make use of the arithmetic operations of phonon [27], which are composed of carrier and uniform blue-sideband π -pulses.

The scheme for projective measurement of $|\downarrow, 0, N\rangle$ is shown in Fig. 4. We first perform the fluorescence detection, if no fluorescence occurs, the qubit state is projected to $|\downarrow\rangle$ [Fig. 4(a)], which removes all the Fock states associated with $|\uparrow\rangle$ due to the imperfections in generating the NOON state. Then we apply one arithmetic subtraction and a π -pulse of carrier transition, which serves as the uniform π -transition of red-sideband in the X mode. The operation transfers the Fock states with $n_X \geq 1$ from $|\downarrow\rangle$ to $|\uparrow\rangle$ [Fig. 4(b)]. If again no fluorescence occurs, these phonon states are eliminated [Fig. 4(c)]. Similarly for the Y mode, by applying N times of successive arithmetic subtractions and then a detection stage, we can eliminate the Fock states with $n_Y < N$ when no fluorescence is detected [Figs. 4(d)(e)]. We note that these operations transfer $|\downarrow, 0, N\rangle$ to $|\downarrow, 0, 0\rangle$. Finally one more subtraction operation and the detection stage are applied [Figs. 4(f)(g)]. If the original state is projected to $|\downarrow, 0, N\rangle$, fluorescence is observed at this detection stage. Altogether, the whole sequence is repeated for 10,000 times and the probability of detecting fluorescence only at the last stage of detection

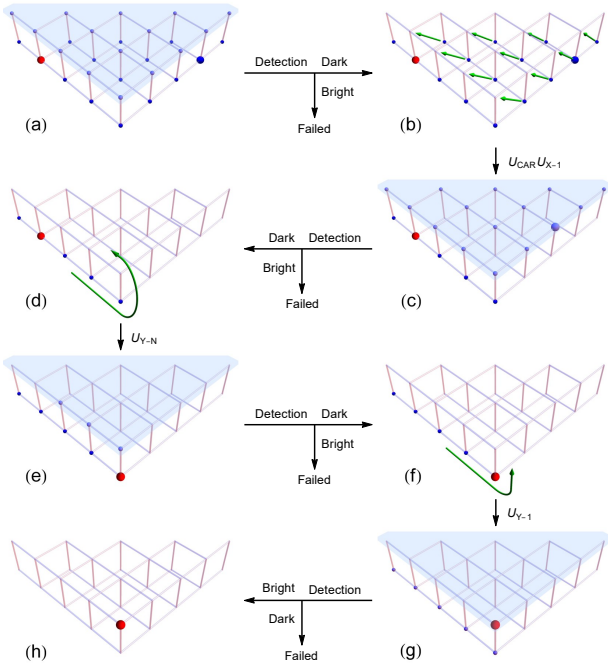


FIG. 4. **Projective measurement of $|\downarrow, 0, N\rangle$.** (a) The state after the generation sequence. The size of the balls indicates its amplitudes on the basis of $|\sigma, n_X, n_Y\rangle$. The target state $|\downarrow, 0, N\rangle$ of the projective measurement is shown in red. (b) After the first detection stage, the Fock states with $n_X \geq 1$ are transferred to $|\uparrow\rangle$ by operations $U_{X-1} = |\uparrow, 0, n_Y\rangle \langle\downarrow, 0, n_Y| + \sum_{n_X > 0} |\downarrow, n_X - 1, n_Y\rangle \langle\downarrow, n_X, n_Y|$ and then $U_{CAR} = |\uparrow\rangle \langle\downarrow| + |\downarrow\rangle \langle\uparrow|$. (c) The second detection stage. (d) The Fock states with $n_Y < N$ are “rolled” to $|\uparrow\rangle$ by operation $U_{Y-N} = \sum_{n_Y < N} |\uparrow, n_X, N - n_Y - 1\rangle \langle\downarrow, n_X, n_Y| + \sum_{n_Y \geq N} |\downarrow, n_X, n_Y - N\rangle \langle\downarrow, n_X, n_Y|$. (e) The third detection stage. (f) Only the target state is brought to $|\uparrow\rangle$. (g) The fourth detection stage. (h) If the system is projected to the target state, then fluorescence is detected in this stage.

is the population of the $|\downarrow, 0, N\rangle$ state, $P_{0,N}$. In a similar manner, $P_{N,0}$ can be measured.

From the results of parity and population measurements, we obtain the fidelity (see Methods, Fidelity Analysis) of the experimental NOON state as

$$F = \frac{1}{2} (C_P + P_{N,0} + P_{0,N}). \quad (7)$$

As shown in Fig. 5(a), the fidelities of the NOON states up to $N = 9$ are clearly larger than 0.5, which confirms these states contain genuine multi-party entanglements.

Quantum Fisher Information

Finally, we observe the Heisenberg scaling of the lower bound of the sensitivity in the phase estimation through the quantum Fisher information (Methods, Quantum Fisher In-

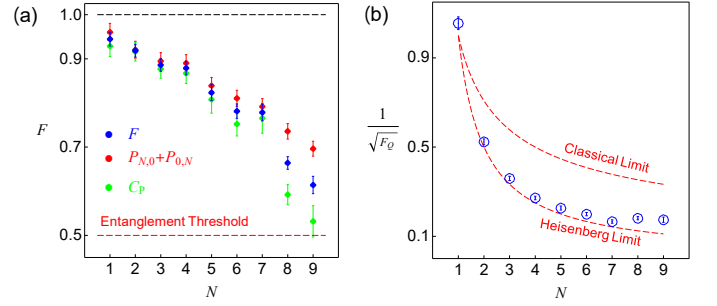


FIG. 5. **Fidelity and quantum Fisher information of the generated states.** (a) The experimental results of fidelity as well as C_P and $P_{N,0} + P_{0,N}$. The error bars of C_P are derived from fitting error and those of $P_{N,0} + P_{0,N}$ from shot-noise error. (b) The quantum Fisher information of the generated states.

formation) of the generated NOON states shown as

$$F_Q = \frac{N^2 C_P^2}{P_{N,0} + P_{0,N}}. \quad (8)$$

The quantum Fisher information provides the best possible precision on a parameter estimation given by $1/\sqrt{F_Q}$ [28, 29], known as the Cramér-Rao bound. For N particles without entanglement, the best possible measurement scales as $1/\sqrt{N}$ and for the NOON state, the lower bound of the precision scales as $1/N$, the Heisenberg limit. As shown in Fig. 5(b), the lower bound of the phase uncertainty, $1/\sqrt{F_Q}$, of our generated states from $N = 2$ to $N = 9$ clearly violate the classical bound and reach to the Heisenberg limit.

DISCUSSION

This scheme of generating NOON states has no principle limit on the number of phonons N . Practically, various imperfections of the system prohibit the increase of the number N . The main problem in our system is the fluctuation of ≈ 10 kHz and the higher drift in the trap frequencies, which induce the increasing errors as the required number of pulses increases as N . The stabilization of the trap frequencies can improve the performances of pulses, which leads to the production of even higher NOON states. Our generic generation and verification scheme of the NOON states can be easily applied to any quantum system that has Jaynes-Cummings interaction including cavity or circuit QED systems [16, 30] and optomechanical systems [31]. We also emphasize that our realization of operating two vibrational modes through a single ion can be the essential component of large scale manipulations on multiple modes of multiple ions including boson sampling of phonons. The series of the demonstrated operations through individual ions together with the phonon number resolving detection [27, 32] enable us to perform phononic boson-sampling.

METHODS

Hamiltonian of the System

In the experiment, we consider only the two radial modes of the ion, so the non-interacting part of the Hamiltonian is:

$$H_0 = \frac{\omega_{\text{HF}}}{2} \sigma_Z + \omega_X a_X^\dagger a_X + \omega_Y a_Y^\dagger a_Y,$$

where ω_{HF} is the frequency splitting of the qubit and ω_X, ω_Y are the trap frequencies of two modes. We denote $\hbar \equiv 1$ for convenience. When the ion is driven by a pair of Raman laser beams with the frequency difference ω , the effective interacting Hamiltonian is written as

$$\begin{aligned} H_1 &= \Omega \cos(\mathbf{k} \cdot \mathbf{r} - \omega t + \phi) \sigma_X, \\ &= \frac{\Omega}{2} e^{i(\phi - \omega t)} e^{i\eta_X(a_X^\dagger + a_X)} e^{i\eta_Y(a_Y^\dagger + a_Y)} \sigma_X + \text{h.c.} \end{aligned}$$

Here η_X and η_Y are the Lamb-Dicke parameters of both vibrational modes. For our system, $\eta_X = 0.0538$, $\eta_Y = 0.0597$, it is within the Lamb-Dicke regime $N < 10$ phonons. After taking an interaction frame with respect to H_0 and Lamb-Dicke approximation together with the rotating wave approximation, the Hamiltonian H_I can be simplified as follows,

$$\begin{aligned} H_C &= \frac{\Omega}{2} (e^{i\phi} \sigma^+ + e^{-i\phi} \sigma^-) \\ H_M &= \frac{i\eta_M \Omega}{2} (e^{i\phi} a_M^\dagger \sigma^+ - e^{-i\phi} a_M \sigma^-), \end{aligned}$$

i.e. carrier transition H_C ($\omega = \omega_{\text{HF}}$) and blue-sideband transition H_M ($\omega = \omega_{\text{HF}} + \omega_M$) for mode $M = X, Y$, respectively. There are also red-sideband transitions for both modes when $\omega = \omega_{\text{HF}} - \omega_M$, which are not used in the experiment.

Pulse Shaping

In the theoretical analysis of the system, many off-resonant terms are neglected. However, in the experiment, these terms can severely degrade the fidelity of the generated state as the required number of pulses increases with the number of phonons. In order to achieve a higher fidelity, we implement the pulse shaping technique to suppress the effect by off-resonant couplings. The electric field of the Raman laser beams at the position of the ion with the ordinary rectangular pulses,

$$E(t) = A \sin[(\omega - \delta)t + \varphi],$$

is changed to a sine-shaped envelope,

$$\begin{aligned} E(t) &= \frac{\pi A}{2} \sin\left[\frac{\pi t}{T}\right] \\ &\times \sin\left[\omega t + \frac{\pi^2 \delta}{8} \left(2\pi t - T \sin\left[\frac{2\pi t}{T}\right]\right) + \varphi\right]. \end{aligned}$$

Step	Operation	Final State
1	$R_X(\pi/2, 0, k_X)$	$ \uparrow, k_X + 1, k_Y\rangle + \downarrow, k_X, k_Y\rangle$
2	$C_Y(k_Y - 1, k_Y)$	$ \downarrow, k_X + 1, k_Y - 1\rangle + \uparrow, k_X, k_Y + 1\rangle$
3	$C_X(k_X + 1, k_X - 1)$	$ \uparrow, k_X + 2, k_Y - 1\rangle + \downarrow, k_X - 1, k_Y + 1\rangle$
4	$C_Y(k_Y - 2, k_Y + 1)$	$ \downarrow, k_X + 2, k_Y - 2\rangle + \uparrow, k_X - 1, k_Y + 1\rangle$
5	$C_X(k_X + 2, k_X - 2)$	$ \uparrow, k_X + 3, k_Y - 2\rangle + \downarrow, k_X - 2, k_Y + 2\rangle$
...
$2k_X$	$C_Y(k_Y - k_X, N - 2)$	$ \downarrow, 2k_X, k_Y - k_X\rangle + \uparrow, 1, N - 1\rangle$
$2k_X + 1$	$C_X(2k_X, 0)$	$ \uparrow, 2k_X + 1, k_Y - k_X\rangle + \downarrow, 0, N - 1\rangle$
For odd N , $k_Y - k_X = 0$ and $2k_X = N - 1$		
$N + 1$	$R_Y(\pi, 0, N - 1), R_C$	$ \downarrow, N, 0\rangle + \downarrow, 0, N\rangle$
For even N , $k_Y - k_X = 1$ and $2k_X = N - 2$		
N	$C_Y(0, N - 1)$	$ \downarrow, N - 1, 0\rangle + \uparrow, 0, N\rangle$
$N + 1$	$R_X(\pi, 0, N - 1), R_C$	$ \downarrow, N, 0\rangle + \downarrow, 0, N\rangle$

TABLE I. Pulse sequence driving $|\downarrow, k_X, k_Y\rangle$ to NOON state $|\downarrow, N, 0\rangle + |\downarrow, 0, N\rangle$

Here A is the amplitude factor, ω and ϕ are the laser frequency and phase resonant to the intended transition, respectively, δ is to compensate the AC-Stark shift effect and T is the duration of the pulse. First, the value of $\omega - \delta$ and the amplitude A are experimentally determined with rectangular pulses and sweeping the driving frequency. The resonant frequency ω is measured by Ramsey method. And finally, the value of δ is once more carefully calibrated with a sine-shaped pulse.

Pulse Sequence

In order to clearly provide a generalized description of the pulse sequence to generate the NOON state, we define the following terms for convenience: R_C denotes a carrier π -pulse and $R_X(\theta, \varphi, n)$ denotes a blue-sideband pulse of the X mode such that the transition between $|\downarrow, n_X, n_Y\rangle$ and $|\uparrow, n_X + 1, n_Y\rangle$ has rotation angle $\theta = \sqrt{n_X + 1} \Omega t$ and φ , $R_Y(\theta, \varphi, n_Y)$ is similarly defined, and

$$C_M(a, b) \equiv R_M(\pi/2, 0, a), R_M(\pi, \pi/2, b), R_M(\pi/2, 0, a)$$

denotes a composite-pulse operation on mode M. With successive blue-sideband pulses of both modes and carrier pulses, the system can be prepared to $|\downarrow, k_X, k_Y\rangle$ with $k_X = \lfloor (N - 1)/2 \rfloor$ and $k_Y = \lfloor N/2 \rfloor$. The remaining part of the sequence is shown in the following Table I. It requires a total number of $5N - 2$ pulses to generate the NOON state from $|\downarrow, 0, 0\rangle$.

Phase Alignment

We measure the phase φ_S of the generated NOON state and then align it to the output mode of $\varphi = 0$. This phase can be measured by scanning the phase φ of the output mode and observing the fluorescence signal of blue-sideband transition at the optimal duration [See Fig. 6(a)(b)]. Fig. 6(c) shows an

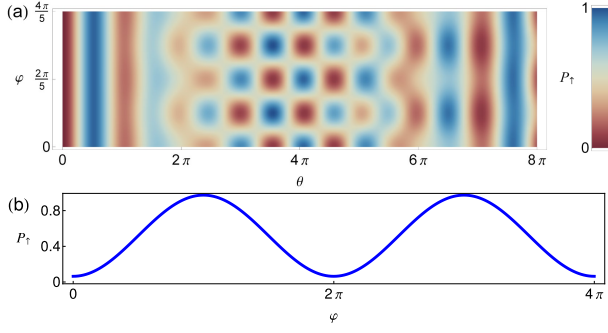


FIG. 6. **Phase measurement for the generated NOON state of $N = 5$.** (a) Theoretical calculation of the dependency of the blue-sideband fluorescence signal on φ . The duration of the excitation is measured in rotation angle $\theta = \Omega_{\text{OT}} t$. The red line indicates the optimal duration, $\theta = 3.55\pi$, for $N = 5$. (b) Theoretical calculation of the fluorescence signal when φ is scanned and θ is set to the optimal. (c) Experimental data of a typical phase scan for $N = 5$, the fitting (red line) indicates an offset of 0.15π .

example of the phase measurement with a result of 0.15π for the case of $N = 5$.

Fidelity Analysis

We assume the density matrix of the generated state to be

$$\begin{aligned} \rho_{\text{exp}} = & P_{N,0} |N, 0\rangle \langle N, 0| + P_{0,N} |0, N\rangle \langle 0, N| \\ & + e^{-iN\phi} \rho_{N0,0N} |N, 0\rangle \langle 0, N| + e^{iN\phi} \rho_{N0,0N} |0, N\rangle \langle N, 0| \\ & + \rho_{\text{noise}}, \end{aligned}$$

where ρ_{noise} stands for the irrelevant part of the density matrix and is independent of ϕ . The fidelity of the generated state to the ideal NOON state $|\psi_{\text{NOON}}\rangle = \frac{1}{\sqrt{2}} (|N, 0\rangle + e^{iN\phi} |0, N\rangle)$ is:

$$\begin{aligned} F = & \langle \psi_{\text{NOON}} | \rho_{\text{exp}} | \psi_{\text{NOON}} \rangle \\ = & \frac{1}{2} (\langle N, 0 | \rho_{\text{exp}} | N, 0 \rangle + \langle 0, N | \rho_{\text{exp}} | 0, N \rangle \\ & + e^{iN\phi} \langle N, 0 | \rho_{\text{exp}} | 0, N \rangle + e^{-iN\phi} \langle 0, N | \rho_{\text{exp}} | N, 0 \rangle) \\ = & \frac{1}{2} [P_{N,0} + P_{0,N} + e^{iN\phi} \rho_{N0,0N} + e^{-iN\phi} \rho_{N0,0N}] \\ = & \frac{1}{2} [P_{N,0} + P_{0,N} + 2\rho_{N0,0N} \cos N(\varphi - \phi)]. \end{aligned}$$

Experimentally setting the phases as $\phi = \varphi = 0$, the fidelity is $F = \frac{1}{2} (P_{N,0} + P_{0,N} + 2\rho_{N0,0N})$. The values of $P_{N,0}$ and $P_{0,N}$ can be directly measured in experiment. The term $2\rho_{N0,0N}$ can be measured by the contrast C_P of the parity oscillation of phonon observed in the output modes. In order to show the relation $2\rho_{N0,0N} \equiv C_P$, we introduce Schwinger's

oscillator model of angular momentum:

$$\begin{aligned} J_X = & \frac{1}{2} (a_X^\dagger a_Y + a_X a_Y^\dagger), \\ J_Y = & \frac{1}{2i} (a_X^\dagger a_Y - a_X a_Y^\dagger), \\ J_Z = & \frac{1}{2} (a_X^\dagger a_X - a_Y^\dagger a_Y). \end{aligned}$$

Then the density matrix of the system can be expressed in the angular momentum basis $|J = N/2, M_z\rangle$ as:

$$\begin{aligned} \rho_{\text{exp}} = & P_{N,0} |J, J\rangle \langle J, J| + P_{0,N} |J, -J\rangle \langle J, -J| \\ & + \rho_{N0,0N} |J, J\rangle \langle J, -J| + \rho_{N0,0N} |J, -J\rangle \langle J, J| \end{aligned}$$

We first consider the form of the parity operator in the X mode,

$$\begin{aligned} \Pi = & \exp [i\pi a_X^\dagger a_X] = \exp \left[\frac{i\pi}{2} (a_X^\dagger a_X - a_Y^\dagger a_Y + N) \right] \\ = & \exp [i\pi J_z] \exp [i\pi J_z]. \end{aligned}$$

With the following beam splitting operator,

$$\begin{aligned} U_{\text{BS}}(\varphi) = & \exp \left[-\frac{i\pi}{4} (a_X^\dagger a_Y e^{i\varphi} + a_X a_Y^\dagger e^{-i\varphi}) \right] \\ = & \exp [i\pi J_X \cos \varphi - J_Y \sin \varphi], \end{aligned}$$

the parity operator can be transformed into the output mode as follows.

$$U_{\text{BS}}^\dagger(\varphi) \Pi U_{\text{BS}}(\varphi) = e^{i\pi N} \sum_{M=-J}^J e^{2iM(\varphi-\pi/2)} |J, M\rangle \langle J, -M|.$$

The parity measured in the output mode is thus

$$\begin{aligned} \langle \Pi(\varphi) \rangle = & \text{Tr} [\rho_{\text{exp}} U_{\text{BS}}^\dagger(\varphi) \Pi U_{\text{BS}}(\varphi)] \\ = & 2\rho_{N0,0N} e^{i\pi N} \cos N(\varphi - \pi/2). \end{aligned}$$

Therefore, the contrast of parity oscillation C_P is thus $2\rho_{N0,0N}$.

Quantum Fisher Information

In order to calculate the quantum Fisher information of the generated state, it is convenient to use the diagonal form of ρ_{exp} ,

$$\rho_{\text{exp}} = \lambda_1 |\psi_1\rangle \langle \psi_1| + \lambda_2 |\psi_2\rangle \langle \psi_2| + \rho_{\text{noise}},$$

where

$$|\psi_1\rangle = \cos \frac{\theta}{2} |N, 0\rangle + e^{iN\phi} \sin \frac{\theta}{2} |0, N\rangle$$

$$|\psi_2\rangle = \sin \frac{\theta}{2} |N, 0\rangle - e^{iN\phi} \cos \frac{\theta}{2} |0, N\rangle$$

$$\rho_{\text{noise}} = \sum_{n>2} \lambda_n |\psi_n\rangle \langle \psi_n|$$

$$P_{N,0} + P_{0,N} = \lambda_1 + \lambda_2$$

$$2\rho_{N0,0N} = |\lambda_1 - \lambda_2| \sin \theta \equiv C_P.$$

The definition of quantum Fisher information is written as

$$F_Q = \text{Tr} [\rho(\phi) A^2]$$

where A is the symmetric logarithmic derivative operator defined by

$$\frac{\partial \rho_{\text{exp}}(\phi)}{\partial \phi} = \frac{1}{2} [A \rho_{\text{exp}}(\phi) + \rho_{\text{exp}}(\phi) A].$$

With this definition, we can calculate the matrix elements of A in the basis expanded by $|\psi_i\rangle$

$$\begin{aligned} \langle \psi_i | \frac{\partial \rho_{\text{exp}}(\phi)}{\partial \phi} | \psi_j \rangle &= \frac{1}{2} (\lambda_j \langle \psi_i | A | \psi_j \rangle + \lambda_i \langle \psi_i | A | \psi_j \rangle) \\ \langle \psi_i | A | \psi_j \rangle &= \frac{2}{\lambda_i + \lambda_j} \langle \psi_i | \frac{\partial \rho_{\text{exp}}(\phi)}{\partial \phi} | \psi_j \rangle. \end{aligned}$$

Note that all λ_n and $|\psi_n\rangle$ with $n > 2$, which form ρ_{noise} , are independent of ϕ , therefore the only non-zero terms are

$$\langle \psi_1 | A | \psi_2 \rangle = -\langle \psi_2 | A | \psi_1 \rangle = i \frac{\lambda_1 - \lambda_2}{\lambda_1 + \lambda_2} N \sin \theta.$$

And hence:

$$F_Q = \lambda_1 \langle \psi_1 | A^2 | \psi_1 \rangle + \lambda_2 \langle \psi_2 | A^2 | \psi_2 \rangle = \frac{N^2 C_P^2}{P_{N,0} + P_{0,N}}$$

Infidelity of the arithmetic subtraction operation

The infidelity of the arithmetic subtraction operation, which consists of a carrier π -pulse and a uniform blue sideband π -transition, is evaluated in experiment as follows. The N times of arithmetic addition operations, which are just arithmetic subtraction operations in reversed order, are applied in the X mode to drive the system from $|\downarrow, 0, 0\rangle$ to $|\downarrow, N, 0\rangle$, then the N times of arithmetic subtraction operations are applied to bring back the state to $|\downarrow, 0, 0\rangle$. By detecting the probability of being in the original state $|\downarrow, 0, 0\rangle$, we evaluate the imperfections of the uniform transfer operations.

We denote the total population of all $|\uparrow, n_X, 0\rangle$ states as p_\uparrow , the total population of all $|\downarrow, n_X, 0\rangle$ states with $n_X > 0$ as p_\downarrow and the population of $|\downarrow, 0, 0\rangle$ with p_0 . The value of p_\uparrow is first determined by fluorescence detection immediately after the sequence of operations. Second, by applying an extra subtraction operation at the end of the sequence, all $|\uparrow, n_X, 0\rangle$ states are transferred to $|\uparrow, n_X + 1, 0\rangle$, $|\downarrow, n_X, 0\rangle$ to $|\downarrow, n_X - 1, 0\rangle$ and $|\downarrow, 0, 0\rangle$ to $|\uparrow, 0, 0\rangle$, so the value of p_\downarrow can be determined by fluorescence detection at this stage, and the value of p_0 is just $1 - p_\uparrow - p_\downarrow$.

This test is performed with $N = 5$ and $N = 9$. For $N = 5$, the sequence contains 10 arithmetic operations and $p_0 = 0.797$, so the fidelity of a single arithmetic operation is $F = 0.797^{1/10} = 0.9776$. And for $N = 9$, $p_0 = 0.667$, and $F = 0.667^{1/18} = 0.9778$. So the fidelity of the sequence transferring $|\downarrow, 9, 0\rangle$ to $|\downarrow, 0, 0\rangle$ is 0.817. We note that the

imperfection of the operation can only decrease the detected population, which only reduces the fidelity of the generated NOON state. However, we do not recalibrate the population that surely provide the lower bound of the fidelity.

ACKNOWLEDGMENT

We thank M. S. Kim, Hyunchul Nha, Chang-Woo Lee, Jeongho Bang, Su-Yong Lee, Chao Shen and Ho-Tsang Ng for the helpful suggestions and discussions. This work was supported by the National Key Research and Development Program of China under Grants No. 2016YFA0301900 (No. 2016YFA0301901), the National Natural Science Foundation of China 11374178, 11574002 and 11504197.

-
- [1] L. Pezzé and A. Smerzi, Phys. Rev. Lett. **102**, 100401 (2009).
 - [2] V. Giovannetti, S. Lloyd, and L. Maccone, Nature Photon. **5**, 222 (2011).
 - [3] B. C. Sanders, Phys. Rev. A **40**, 2417 (1989).
 - [4] P. Kok, H. Lee, and J. P. Dowling, Phys. Rev. A **65**, 052104 (2002).
 - [5] M. W. Mitchell, J. S. Lundeen, and A. M. Steinberg, Nature **429**, 161 (2004).
 - [6] P. Walther, J.-W. Pan, M. Aspelmeyer, R. Ursin, S. Gasparoni, and A. Zeilinger, Nature **429**, 158 (2004).
 - [7] T. Nagata, R. Okamoto, J. L. O'Brien, K. Sasaki, and S. Takeuchi, Science **316**, 726 (2007).
 - [8] J. P. Dowling, Contemporary Physics **49**, 125 (2008).
 - [9] I. Afek, O. Ambar, and Y. Silberberg, Science **328**, 879 (2010).
 - [10] F. Wolfgramm, C. Vitelli, F. A. Beduini, N. Godbout, and M. W. Mitchell, Nature Photon. **7**, 28 (2013).
 - [11] G.-Q. Liu, Y.-R. Zhang, Y.-C. Chang, J.-D. Yue, H. Fan, and X.-Y. Pan, Nat. Commun. **6**, 6726 (2015).
 - [12] X.-L. Wang, L.-K. Chen, W. Li, H.-L. Huang, C. Liu, C. Chen, Y.-H. Luo, Z.-E. Su, D. Wu, Z.-D. Li, H. Lu, Y. Hu, X. Jiang, C.-Z. Peng, L. Li, N.-L. Liu, Y.-A. Chen, C.-Y. Lu, and J.-W. Pan, arXiv:1605.8547 (2016).
 - [13] T. Monz, P. Schindler, J. T. Barreiro, M. Chwalla, D. Nigg, W. A. Coish, M. Harlander, W. Hansel, M. Hennrich, and R. Blatt, Phys. Rev. Lett. **106**, 130506 (2011).
 - [14] J. A. Jones, S. D. Karlen, J. Fitzsimons, A. Ardavan, S. C. Benjamin, G. A. D. Briggs, and J. J. L. Morton, Sciences **324**, 1166 (2009).
 - [15] Y.-A. Chen, X.-H. Bao, Z.-S. Yuan, S. Chen, B. Zhao, and J.-W. Pan, Phys. Rev. Lett. **104**, 043601 (2010).
 - [16] H. Wang, M. Mariani, R. C. Bialczak, M. Lenander, E. Lucero, M. Neeley, A. D. O'Connell, D. Sank, M. Weides, J. Wenner, T. Yamamoto, Y. Yin, J. Zhao, J. M. Martinis, and A. N. Cleland, Phys. Rev. Lett. **106**, 060401 (2011).
 - [17] D. Meekhof, C. Monroe, B. King, W. Itano, and D. Wineland, Phys. Rev. Lett. **76**, 1796 (1996).
 - [18] D. Leibfried, R. Blatt, C. Monroe, and D. Wineland, Rev. Mod. Phys. **75**, 281 (2003).
 - [19] D. Porras and J. I. Cirac, Phys. Rev. Lett. **93**, 263602 (2004).
 - [20] K. Toyoda, Y. Matsuno, A. Noguchi, S. Haze, and S. Urabe, Phys. Rev. Lett. **111**, 160501 (2013).

- [21] C. Shen, Z. Zhang, and L. M. Duan, Phys. Rev. Lett. **112**, 050504 (2014).
- [22] L. Ortiz-Gutiérrez, B. Gabrielly, L. F. M. noz, K. a. T. Pereira, J. G. Filgueiras, and A. S. Villar, arXiv:1603.00065 (2016).
- [23] K. Toyoda, R. Hiji, A. Noguchi, and S. Urabe, Nature **527**, 74 (2015).
- [24] J. M. Raimond, M. Brune, and S. Haroche, Rev. Mod. Phys. **73**, 565 (2001).
- [25] D. Hayes, D. N. Matsukevich, P. Maunz, D. Hucul, Q. Quraishi, S. Olmschenk, W. Campbell, J. Mizrahi, C. Senko, and C. Monroe, Phys. Rev. Lett. **104**, 140501 (2010).
- [26] F. Schmidt-Kaler, H. Haffner, M. Riebe, S. Gulde, G. P. T. Lancaster, T. Deuschle, C. Becher, C. F. Roos, J. Eschner, and R. Blatt, Nature **422**, 408 (2003).
- [27] M. Um, J. Zhang, D. Lv, Y. Lu, S. An, J.-N. Zhang, H. Nha, M. S. Kim, and K. Kim, Nat. Commun. **7**, 11410 (2016).
- [28] S. L. Braunstein and C. M. Caves, Phys. Rev. Lett. **72**, 3439 (1994).
- [29] J. J. Cooper and J. A. Dunningham, New J. Phys. **13**, 115003 (2011).
- [30] Q.-P. Su, C.-P. Yang, and S.-B. Zheng, Sci. Rep. **40**, 2417 (2014).
- [31] M. Aspelmeyer, T. J. Kippenberg, and F. Marquardt, Rev. Mod. Phys. **86**, 1391 (2014).
- [32] S. An, J. N. Zhang, M. Um, D. Lv, Y. Lu, J. Zhang, Z.-Q. Yin, H. T. Quan, and K. Kim, Nature Phys. **11**, 193 (2015).